

Article

Study on Redistribution of Internal Force and Plastic Hinge Development of Mountainous Building Structures with Foundations at Two Different Elevations

Yangyang Tang ¹, Yingmin Li ¹, Baolong Jiang ¹, Liping Wang ² and Shuyan Ji ^{3,*}¹ School of Civil Engineering, Chongqing University, Chongqing 400045, China; tyyang90@126.com (Y.T.)² School of Civil Engineering and Architecture, Chongqing University of Science & Technology, Chongqing 401331, China³ School of Management Science and Real Estate, Chongqing University, Chongqing 400045, China

* Correspondence: jishuyan_cqu@126.com

Abstract: This study was conducted to study the redistribution of internal force and the development of the plastic hinge of an MBS with foundations at two different elevations considering the torsional effect. The results indicate that the redistribution of the base shear of MBS is evident at different embedding ends, and the redistribution of story shear on different floors also took place. The redistribution of the shear force of columns is different at the upper- and lower-embedding sides, and the internal force redistribution is more prominent along the slope direction. Consequently, the redistribution of the internal force of MBS should be considered in practical seismic design. Furthermore, the damage of MBS is transferred from the floors above the upper-embedding end to the floors under the upper-embedding end with the increase in the seismic intensity, where the elements at the floors above the upper-embedding end suffer the most serious damage, and the damage is unevenly distributed in the upper-embedding story and the adjacent upper story. The lower-embedding column is more prone to hinge across the slope direction because of the torsional effect. With γ_{intra} changes, the redistributions of the shear force of the base, story, and column are different. A larger γ_{intra} would result in a weaker redistribution of base shear. The redistribution of the story shear of the 1st floor and its columns along the slope direction shows an increasing-decreasing tendency with the increase in γ_{intra} , and the redistribution is the most serious when γ_{intra} is 0.4. While across the slope direction, the redistribution of the story shear tends to be weakened as γ_{intra} increases. The forming of the plastic hinge of single-frames along the slope direction is related to γ_{intra} and γ_{non} , especially the damage of the upper-embedding columns. The torsional effect has a significant influence on the damage of the single-frames across the slope direction. Some measures should be taken to improve the bearing capacity of the upper embedding columns and columns on floors under the upper-embedding end, as well as the drift ductility of the upper-embedding columns.



Citation: Tang, Y.; Li, Y.; Jiang, B.; Wang, L.; Ji, S. Study on Redistribution of Internal Force and Plastic Hinge Development of Mountainous Building Structures with Foundations at Two Different Elevations. *Buildings* **2023**, *13*, 909. <https://doi.org/10.3390/buildings13040909>

Academic Editor: Krishanu Roy

Received: 21 February 2023

Revised: 26 March 2023

Accepted: 27 March 2023

Published: 30 March 2023

Keywords: mountainous building structure; redistribution of internal force; plastic hinge; torsional effect; shear force



Copyright: © 2023 by the authors. Licensee MDPI, Basel, Switzerland. This article is an open access article distributed under the terms and conditions of the Creative Commons Attribution (CC BY) license (<https://creativecommons.org/licenses/by/4.0/>).

1. Introduction

The mountainous building structure (MBS) on the slope is a kind of structure supported by foundations at different elevations to adapt to the site conditions, resulting in different dynamic responses and seismic damage mechanisms from conventional ones due to the changes in the distribution of lateral stiffness in both the vertical and planar directions. It has been verified in the Wenchuan Earthquake [1] and the Sikkim Earthquake [2,3] that MBS experienced peculiar and more severe seismic damage.

In recent years, the seismic response of MBS has made some progress in research. Surana et al. [4,5] conducted extensive field surveys in two test bed cities situated in the Himalayan state of Uttarakhand in India to develop a comprehensive building stock

inventory and investigated the seismic fragility using a numerical study, discovering that buildings in hilly regions are significantly more vulnerable to earthquake, and the collapse occurs due to the combined effect of shear failure of short columns and flexural failure of beams and columns in the story just above the uppermost foundation level. Birajdar et al. [6], Subhash et al. [7] investigated the seismic response of structures with different configurations. The results suggested that the seismic performance of MBS is poorer than that of the set-back structure, and the torsional effect of MBS is more prominent. Tang et al. [8] compared the dynamic response of an MBS supported by foundations with two different elevations and two corresponding conventional frame structures from the linear elasticity stage to plasticity and failure stages, and results show that the force, deformation, and plastic hinges of MBS are different from that of conventional structures, and there is an obvious difference along and across the slope direction. Studies have demonstrated that the seismic response of the MBS differs from that of ordinary structures, and the MBS suffers from severe torsional effects under earthquakes.

Meanwhile, there are many studies on the influence of different factors on the structural dynamic response. Literature [9–11] investigated the influence of non-structural factors such as soil-structure interaction, nonuniform seismic excitation, and the characteristics of ground motions. In terms of the influence of structural factors, Aggarwal et al. [12] investigated the effect of one or more open stories in reinforced concrete hilly buildings and discovered that the building with the open story at the uppermost foundation level is the most vulnerable under earthquake excitation. Thakur et al. [13] carried out a study on the influence of the rooftop telecommunication tower on set back-step back building resting on different ground slopes, finding that the tower position and the slope's gradient would affect the safety of the tower. Li et al. [14] proposed three types of steel brace arrangement for frame structures supported by foundations with two different elevations, and results of the quasi-static test indicate that setting V-shaped braces can significantly reduce the damage degree of the upper embedding columns and change the phenomenon of locally severe damage of the split-foundation frame structure. Surana et al. [15] assessed the damage probability matrices of hill-side RC buildings, and the result showed that the choice of the ground-motion intensity measures and the structural configuration type show quite significant effects on the resulted damage probabilities of different damage states. Besides, Surana et al. [16] obtained the floor response and proposed and validated the simple floor spectral amplification functions. Jain et al. [17] investigated the seismic response of acceleration-sensitive non-structural components, and proposed floor displacement-based models to compute the torsional amplification factors.

Research on seismic failure mechanism of structures is necessary for a reasonable seismic design. The numerical simulations [18,19] and experimental studies [20] on the seismic failure mechanism of the MBS have proceeded and found that upper-embedding columns were damaged seriously, and a "half-story mechanism" is likely to occur. However, the research object of these studies is mainly the plan along the slope direction of the MBS, and the pushover analysis method is always adopted. Li et al. [21] conducted shaking table tests to compare the dynamic response and failure characteristics of a frame structure supported by foundations with two different elevations from those of a corresponding conventional structure, and the results indicated that the column hinge first appears at the end of the upper embedding column, then transfers to the floors under the upper embedding end with the increase in earthquake intensity. Meanwhile, the torsional effect of the former frame structure is remarkable, and the damage of the bottom corner column ends increases significantly. Xu et al. [22] investigated the seismic performance and improvements of split-foundation buildings across the slope direction using pushover analysis with the load mode of the first mode, and the results indicated that the upper-embedding columns were the weakest part of the structure, and the floors under the upper-embedding end were destroyed in succession. The results of these studies all demonstrate the special seismic failure mechanism of the MBS, while most of them focus on the plan along the slope direction and its final damage state, also, the results on structural torsional effect

may be inaccurate, so the detailed damage process needs further research and the torsional effect should be analyzed reasonably.

As the damage of the structure changes, the redistribution of the internal force of the members has a certain regularity, which can reflect the damage mechanism of the structure to a certain extent. Most studies aim at the internal force redistribution of continuous beams or single members [23,24], which reveals the mechanism of internal force redistribution at the member and interface levels. Also, the influence of differential consolidation settlement of the foundation on the redistribution of internal force of structures is analyzed to provide a reference for the reinforcement [25]. For the MBS, Ji et al. [26] studied the base stress distribution by overall finite element models containing soil and structure established using ANSYS, finding that the negative compression zone is greater than the positive one when the overturning load increases. Xu et al. [19] observed the shear distribution of each ground column in an elastic state, finding the shear force of the upper ground columns is generally larger than that of the lower ground columns. Wu [27] investigated the distribution of the shear force of columns at the upper embedding story, revealing the significant redistribution of the shear force of columns in this story. Jiang et al. [28] noticed that the axial beam compression and tension are larger and researched the impact of axial beam tension on joint shear capacity, and the results indicated that the shear capacity of the joint may be lost when tension is experienced. There is not much research on the structural force, and the torsion of the structure is neglected.

Although there are so many studies on the seismic response and failure characteristics of the structure supported by foundations with different elevations, most studies are on two-dimensional models along the slope direction, which ignores the torsional effect. The redistribution of internal force is rarely noticed, and previous studies have focused on the internal force of the upper embedding columns. Studies on force characteristics and damage path of MBS consider torsional effects are scarce. Hence, the present research addresses the behavior of three-dimensional MBS, subjected to earthquake waves. The study includes the force and plastic hinges of three-dimensional MBS. Also, the effect of the stiffness distribution between the upper- and the lower- embedding sides of the upper-embedding story on redistribution of internal force and plastic hinge development is studied to improve the seismic performance of the MBS. The main purpose of the study is to obtain the redistribution of internal force and plastic hinge development of three-dimensional MBS, and the results will be a reference for seismic design and reinforcement of MBSs.

2. Object and Methodology

Currently, the MBS with two different elevations is one of the main subjects of study, and it will be the object of this study. Figure 1 shows the typical MBS, and the terminology for each position of the model is also presented.

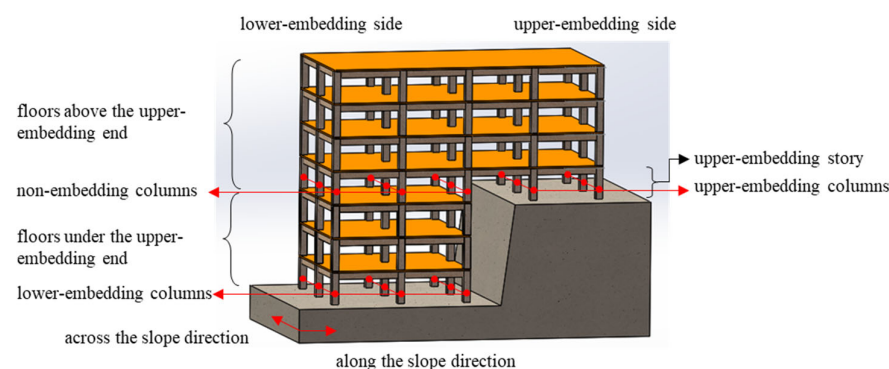


Figure 1. Schematic diagram of the typical MBS and the terminology of each position.

A detailed case study is carried out by nonlinear dynamic history analysis using 3 groups of natural waves and 1 group of artificial waves on a typical RC MBS with two different elevations. The structural response in the form of base shear, story shear, column shear, and plastic hinges are obtained, and the laws of redistribution of internal force and damage path are discussed. For subsequent parameter analysis, MBSs with different structural arrangements are established and analyzed, and the influence of structural configuration is investigated. The flow chart is shown in Figure 2.

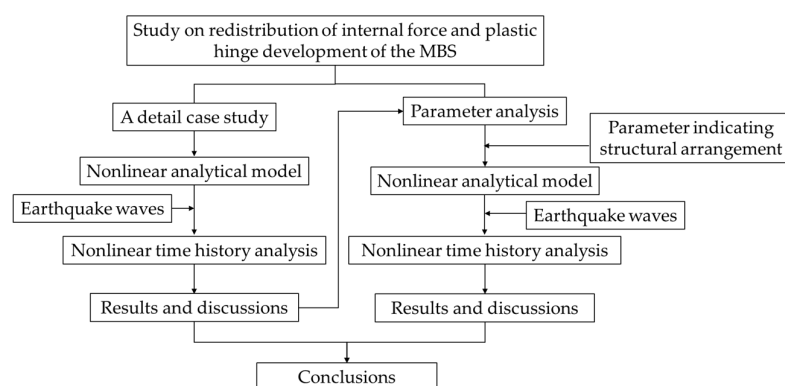


Figure 2. The flow chart of the present work.

3. Seismic Response Analysis of an Example MBS Model

In this section, an RC-frame MBS supported by foundations with two different elevations is built as the example model. The distribution and redistribution of shear force are obtained, and the distribution and development of plastic hinges are investigated. The failure path and mechanism of the structure will be discussed.

3.1. Analytical Model and Earthquake Waves

Figure 3 shows an RC-frame MBS with 3×2 bays and 6 stories supported by foundations with different elevations, named M0. The x -axis is along the slope direction, and the y -axis is across the slope direction.

The floor height is set constant at 3.0 m, and the bay width is 6.0 m in both horizontal directions. The cross sections of columns and beams are respectively $600 \text{ mm} \times 600 \text{ mm}$ and $300 \text{ mm} \times 600 \text{ mm}$. The thickness of the floor slab is 140 mm to meet the deflection requirements, and there are no secondary beams. The additional uniform dead load and the uniform live load are respectively set as 1.5 kN/m^2 and 2.0 kN/m^2 for all floors. The linear dead load of the infilled walls is 9 kN/m on all beams from the 1st floor to the 5th floor, and the linear dead load on the surrounding beams of the top floor is 3 kN/m . HRB400 rebar and C30 concrete are used.

It's assumed that the basic fortification intensity of the structures is Intensity 8, the site type is II, and the predominant period T_g is 0.35 s according to GB 50011-2010 [29]. Rebars of upper-embedding columns and columns at the lower-embedding side of the 4th floor are designed by the seismic bearing capacity, and rebars of other columns are determined based on the minimum rebar ratio.

OpenSees was used for the nonlinear analysis of the 3D model using the Concrete02 model for concrete. The strength deterioration model based on effective hysteresis energy dissipation was adopted for the rebar, whose accuracy in modeling has been verified [30,31]. The sections of the beam and column are fiber sections. The Nonlinear-Beam-Column Element, a distributed plasticity element based on the finite element flexibility method, is chosen to simulate the beam and column elements. At the top of the upper-embedding columns, the Zero-length element is introduced in series with the beam-column element, and the load-displacement relationship of the shear spring is defined in terms of the Shear Limit Curve and Limit State Material. Axial Limit Curve and Limit State Material are used to define the load-displacement relationship of the axial spring to take account of the

bending, shear and axial effects of the member [32]. Rayleigh damping with a damping ratio of 5% is used in the analysis of time history.

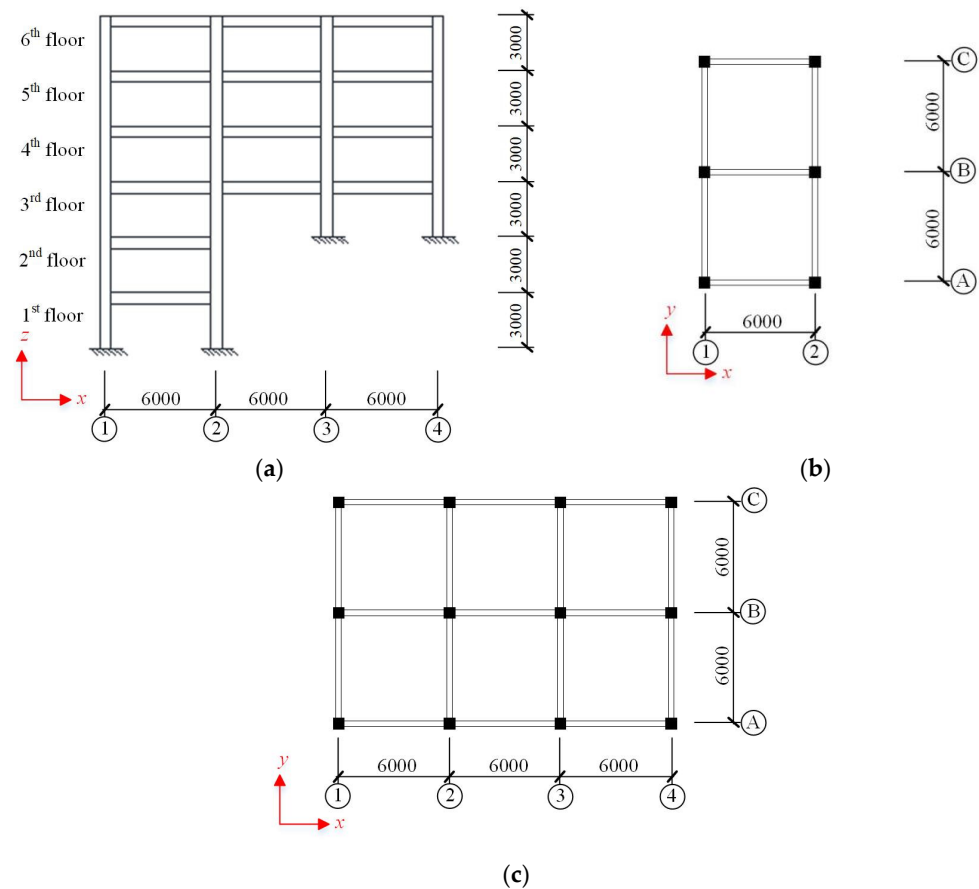


Figure 3. Layout of a typical MBS: (a) Elevation view; (b) Plan view from the 1st to 2nd floor; (c) Plan view from the 3rd to 6th floor.

Three groups of natural earthquake waves are selected considering the natural vibration period of the MBS and the site conditions, as shown in Table 1, where $a_{PG,x}$ represents the peak acceleration on the x -axis. In addition, one group of artificial waves was created according to GB 50011-2010. The elastic amplification factor spectra for 5% damping are shown in Figure 4. The used $a_{PG,x}$ of the natural and artificial waves are 0.07 g, 0.2 g, 0.4 g, 0.51 g and 0.62 g are applied to the structure to represent the frequent earthquake, moderate earthquake, rare earthquake of Intensity 8, rare earthquake of Intensity 8.5 and rare earthquake of Intensity 9, respectively.

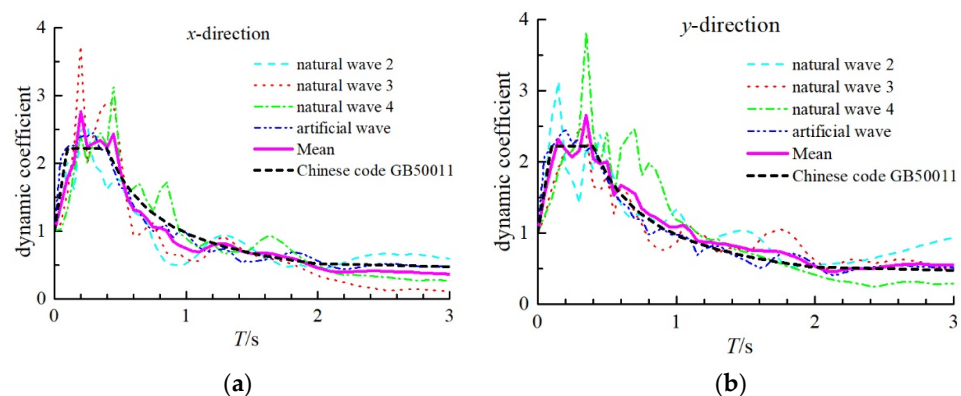


Figure 4. Elastic amplification factor spectra for 5% damping: (a) x -direction; (b) y -direction.

Table 1. Information of natural earthquake waves.

ID	Year	Earthquake Name	Magnitude	Station Name	V_{s30}^1/gal	$a_{PG,x}/\text{gal}$
2	2008	Iwate-Miyagi Nairiku Earthquake	6.9	Kami Miyagi	478	153
3	1994	Northridge Earthquake	6.7	Fairview Ave,	291	123
4	1952	Kern County Earthquake	7.3	Taft Lincoln School Tunnel	385	176

¹ V_{s30} represents the equivalent shear wave velocity at a calculated depth of 30 m.

3.2. Internal Force and Its Redistribution

The internal force of the structure at the moment of maximum base shear is selected to analyze the distribution and redistribution of base shear, story shear, and elements shear.

3.2.1. Base Shear

The base shear of MBS includes the shear forces of both the upper-embedding and the lower-embedding columns. When the base shear reaches the maximum value, the proportion of the base shear of lower-embedding columns is listed in Table 2. For $a_{PG,x} = 0.07\text{ g}$, the proportion of the base shear borne by lower embedding columns is 0.10 and 0.22 in the two directions, this shows that the most of the base shear are borne by upper-embedding columns, which is consistent with the results in literature [19]. The proportion of the base shear of lower-embedding columns displays a low value of 5% along the slope direction, while that reaches a much higher value of 10%. This suggests that the actual stiffness of the upper-embedding columns and lower-embedding columns are different, despite the same section and number of columns. For lower-embedding columns across the slope direction, their actual stiffness is larger than those along the slope direction. As a consequence, when suffering a strong earthquake with high intensity, the lateral stiffness of upper-embedding columns would be degraded, the distribution of base shear of the MBS could be changed, and lower-embedding columns should bear more base shear. Moreover, the proportions of the base shear of lower-embedding columns in the two directions of the slope tend to increase, where the increment is more prominent along the slope direction, revealing that the stiffness degradation of upper-embedding columns and the transfer of structural damage to the floors under the end of the upper-embedding columns are enhanced. It can be seen that the base shear of the MBS has been significantly redistributed at different embedding ends, and the redistribution degree of base shear is more notable along the slope direction.

Table 2. The proportion of the base shear borne by lower embedding columns.

Record ID	Along the Direction of the Slope					Across the Slope Direction				
	0.07 g	0.2 g	0.4 g	0.51 g	0.62 g	0.07 g	0.2 g	0.4 g	0.51 g	0.62 g
Natural wave 2	0.10	0.12	0.15	0.21	0.21	0.22	0.31	0.29	0.29	0.29
Natural wave 3	0.06	0.06	0.07	0.17	0.17	0.27	0.32	0.25	0.32	0.27
Natural wave 4	0.09	0.11	0.13	0.21	0.21	0.28	0.27	0.32	0.33	0.33
Artificial wave	0.05	0.05	0.11	0.15	0.26	0.23	0.27	0.28	0.28	0.28

3.2.2. Story Shear

The distribution patterns of the story shear of the MBS are very similar under different seismic waves. Figure 5 shows the story shear of the MBS suffered by Natural-wave 2 at the time when the base shear reaches its maximum value. This shows that for both directions of the slope, the story shear of the under-part of the upper-embedding end decreases sharply, and part of the story shear has been transferred to the foundation instead of the floors under the upper-embedding end. It has been clarified by previous studies [3,8]. With the increase in the earthquake intensity, the story shear of floors under the upper-embedding ends increases generally. For the floors above the upper-embedding ends, the story shear increase in both horizontal directions. When $a_{PG,x}$ is 0.2 g, the story force is basically

proportional to that with 0.07 g of $a_{PG,x}$, which shows the MBS is still in an elastic state, or in a slight elastic-plastic state, and its dynamic properties do not change much. Nevertheless, for $a_{PG,x} \geq 0.4$ g, the story shear of partial floors is relatively reduced, especially when $a_{PG,x}$ reaches 0.62 g. This is related to the stiffness degradation of the MBS, and the maximum story shear and the maximum base shear of floors are not occurring simultaneously.

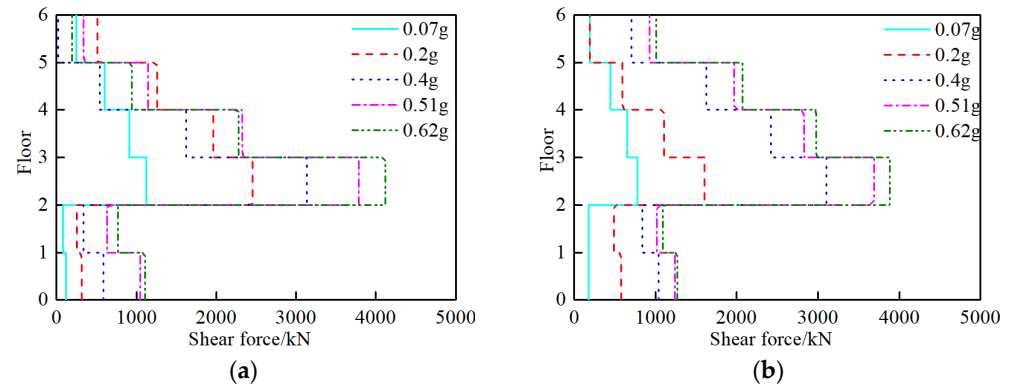


Figure 5. Distribution of story shear at the moment of maximum base shear: (a) Along the slope direction; (b) Across the slope direction.

$\lambda = V/V_{0.07g}$ was used to characterize the amplification of the shear force of the MBS, stories, or the elements under a strong earthquake, where $V_{0.07g}$ denotes the maximum shear force under an $a_{PG,x}$ of 0.07 g, and V means the maximum shear force.

Figure 6 shows the λ of the MBS under Natural-wave 2. This clearly shows that the λ of the floors above the upper-embedding end varies slightly with the increase in $a_{PG,x}$. For instance, the λ of each floor is similar ranging from 2.0 to 3.0 when $a_{PG,x} = 0.2$ g in both directions of the slope. When $a_{PG,x} \geq 0.4$ g, the λ of the floors under the upper-embedding end along the slope direction become obviously larger than those above the upper-embedding end, as shown in Figure 6a. This indicates that the story shear of the MBS has been redistributed at different floors. In contrast, the changes of λ of all the floors across the slope direction (Figure 6b) are less obvious compared with Figure 6a, which reveals that more attention should be paid on the redistribution of story shear along the slope direction of an MBS.

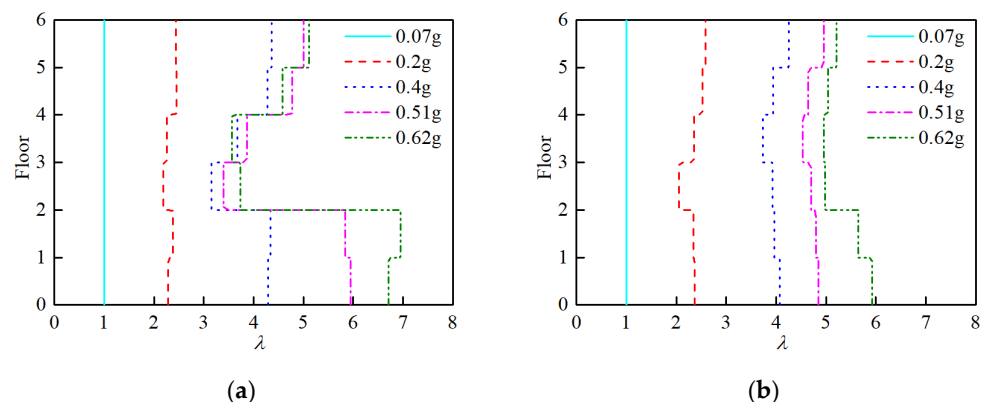


Figure 6. The λ of each floor at the moment of maximum base shear: (a) Along the slope direction; (b) Across the slope direction.

3.2.3. Column Shear

Figures 7 and 8 show the column shear in the two directions of the slope under the maximum base shear, where the shear force is the sum of the shear of columns at Axis 1, 2, 3, and 4. As can be seen from Figure 7a,b, most of the story shear of the upper-embedding story has been borne by upper-embedding columns, and the directions of the

shear force of columns at Axis 1 or Axis 2 may be opposite to that of upper-embedding columns. Consequently, the relative deformation of the columns at the lower-embedding side and upper embedding-side on the upper-embedding story will be opposite owing to the relationship between force and deformation. Moreover, the rotation and relative deformation of columns at the lower-embedding side are smaller than those of columns at the upper-embedding side. On the adjacent upper floor of the upper-embedding story, the shear forces of the columns at Axis 1 and Axis 2 are greater than those at Axis 3 and Axis 4, which is contrary to the results of the upper-embedding story. Moreover, the shear forces of columns under the upper-embedding ends are relatively small under $a_{PG,x} = 0.07\text{ g}$, but increase obviously when $a_{PG,x}$ is 0.62 g, which is consistent with the redistribution of the story shear of floors.

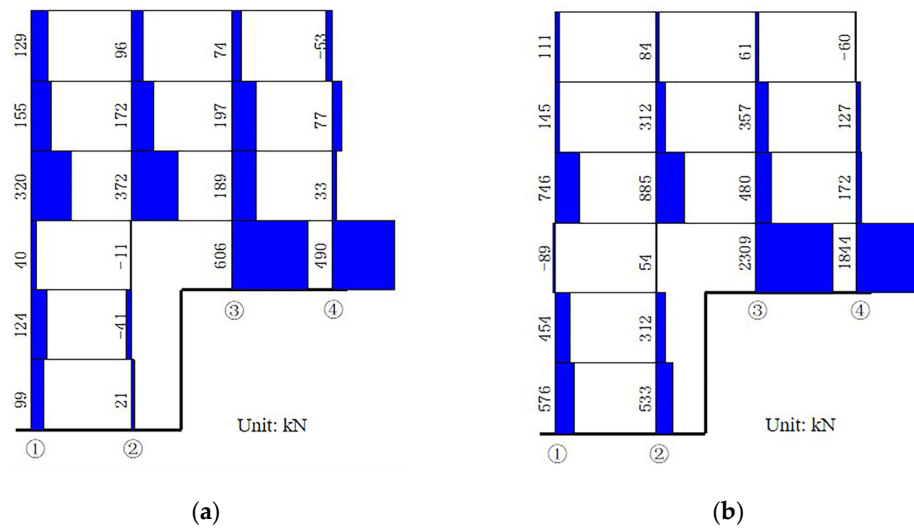


Figure 7. The column shear along the slope direction at the time of maximum base shear: (a) $a_{PG,x} = 0.07\text{ g}$; (b) $a_{PG,x} = 0.62\text{ g}$.

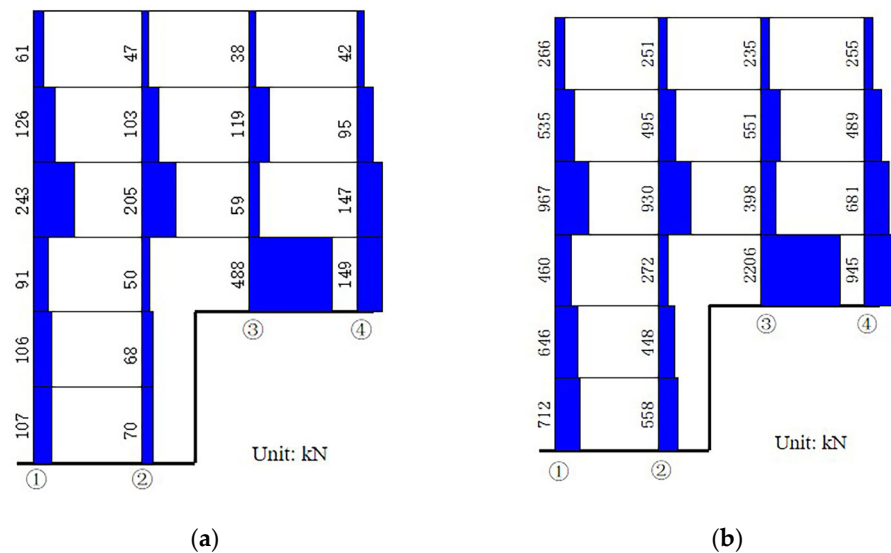


Figure 8. The column shear across the slope direction at the time of maximum base shear: (a) $a_{PG,x} = 0.07\text{ g}$; (b) $a_{PG,x} = 0.62\text{ g}$.

Figure 8a,b show the column shear across the slope direction. For the upper-embedding story, the shear forces of columns at Axis 1 and Axis 2 are lower, and the proportion of the shear force of these columns is increased compared with those along the slope direction. It can be found that the shear force of the columns at Axis 1 and Axis 3 are commonly larger

than those at Axis 2 and Axis 4, and the increase in the seismic intensity has not caused obvious changes in the distribution of the shear force of columns.

Figures 9 and 10 show the λ of columns at Axis 1, 2, 3, and 4 in the two directions of the slope. This clearly shows that the redistributing pattern of internal force differs in two different directions. For the column shear along the slope direction, the changes in λ of the columns at Axis 1 and Axis 2 are different from those at Axis 3 and Axis 4. For the columns at the lower-embedding side, e.g., Axis 1 and Axis 2, the λ of columns on the 3rd floor is larger than that on the 4th floor. In contrast, the λ of columns on the 3rd floor at the upper-embedding side is less than that of columns on the 4th floor. Meanwhile, the λ of columns on the 3rd floor at the lower-embedding side is greater than that at the upper-embedding side. The results show that the stiffness degradation of columns on the 3rd and 4th floor differs as the columns at the lower-embedding side of the 4th floor lose more stiffness. Moreover, λ of columns of the lower-embedding end of the 1st floor is obviously greater than that of the adjacent upper floor. Under a high-intensity earthquake, the redistribution of the internal force occurs, and the upper-embedding columns are seriously damaged with great stiffness reductions, where the non-embedding columns bear more shear and the lower-embedding columns will be loaded with more base shear.

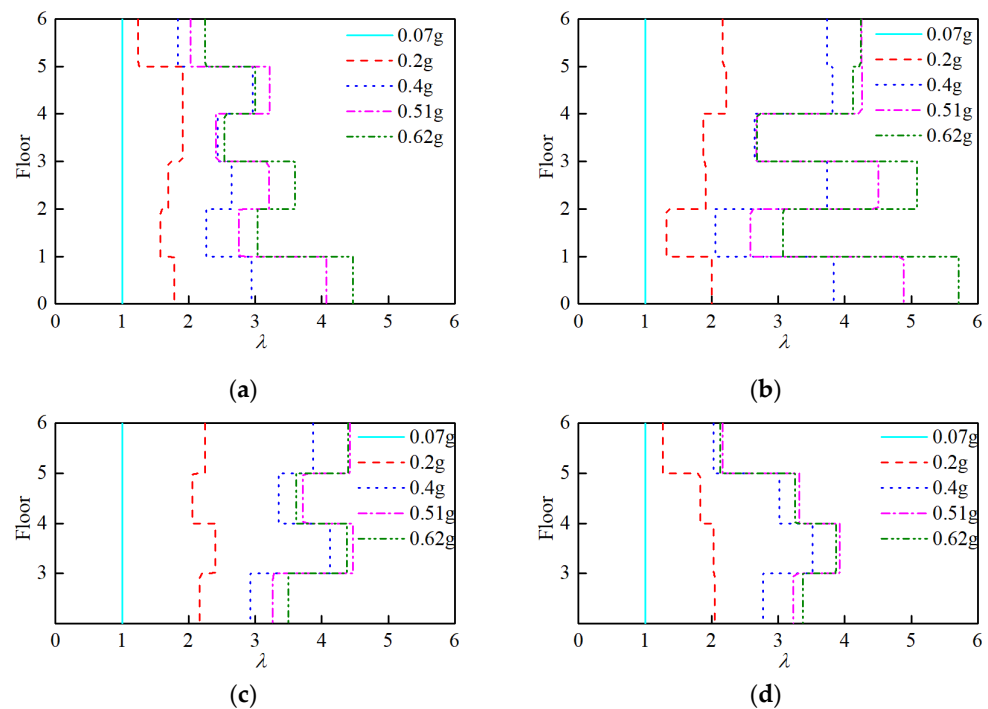


Figure 9. The λ of column along the slope direction: (a) Axis 1; (b) Axis 2; (c) Axis 3; (d) Axis 4.

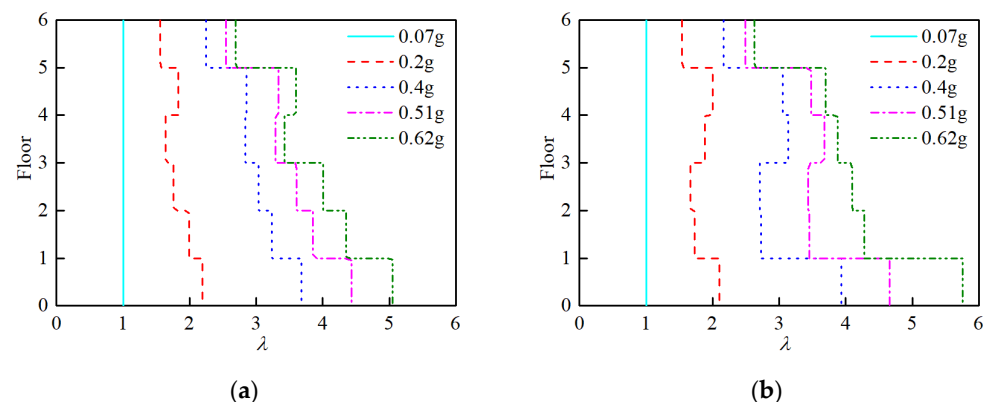


Figure 10. Cont.

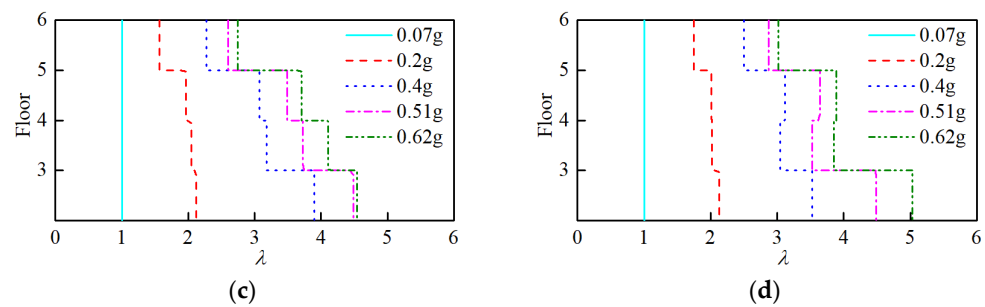


Figure 10. The λ of column across the slope direction: (a) Axis 1; (b) Axis 2; (c) Axis 3; (d) Axis 4.

It can be seen that some measures should be considered in the seismic design of the upper-embedding columns to increase the load-bearing capacity to avoid serious damage under earthquakes. The shear bearing capacity of the vertical members of floors under the upper-embedding end can be thus increased to bear the increased shear force.

3.3. Distribution and Development of Plastic Hinges

To better interpret the formation of plastic hinges due to bending damage of the elements of MBS, the ductility demand coefficient of sectional curvature μ_ϕ was adopted to indicate the degree of the plastic hinge, as expressed by Equation (1).

$$\mu_\phi = \frac{\phi}{\phi_y} \quad (1)$$

where ϕ and ϕ_y are the maximum curvature and yield curvature of the end of elements, respectively. Plastic hinges could be formed when $\mu_\phi \geq 1$.

Figures 11 and 12 show the plastic hinges of the MBS under natural wave 2 with $a_{PG,x} = 0.4 \text{ g}$ and 0.62 g , respectively, where μ_ϕ is marked. As can be seen from Figure 11, for the single-frame across the slope direction, e.g., those single-frames at Axis 1, 2, 3, and 4, the beam hinges mainly form on the 3rd and 4th floors. Moreover, beam hinges can also be found on the 2nd floor in outer frames at the lower-embedding side. Column hinges appear on the 4th and 5th floor of the lower-embedding side single-frame, and the number and degree of column hinges at Axis 1 are larger than those at Axis 2 due to the torsional effect. In addition, column hinges appear at the bottom of upper-embedding columns at Axis 3. For the single-frames along the slope direction, e.g., single-frames at Axis A, B, and C, the beam hinges and column hinges mainly appear at the 3rd to 5th floor, and no plastic hinge can be found at the end of the elements under the upper-embedding end. In the upper-embedding story, column hinges develop at the end of upper-embedding columns, and non-embedding columns are not damaged. On the 4th floor, μ_ϕ at the bottom of the columns at Axis 1 and 2 is obviously greater than the others on this floor.

It can be summarized that column hinges at the end of the embedding column are inclined to be formed at the upper-embedding columns of side single-frame along the slope direction and the upper-embedding columns of the inner single-frame across the slope direction. The distribution of column hinges of the upper-embedding story and the adjacent upper floor are not uniform. The column at the upper-embedding side is hinged in the upper embedding story, while the degree of column hinges at lower embedding side of the adjacent upper floor is greater. The damage of elements under the upper-embedding end is obviously weaker than those above the upper-embedding end. The structural damage is similar to the “half-story mechanism” presented by Xu et al. [18].

As can be seen from Figure 12, the number and degree of plastic hinges at the ends of the beam and column increase with the seismic intensity up to 0.62 g . For the single-frames across the slope direction, the degrees of beam hinges on the 3rd and 4th floors are higher than the other beams, and the beams at the floors under the upper-embedding end are hinged. In addition, the plastic hinges appear at the bottom of lower-embedding columns, and the degree of plastic hinges at embedding-columns at Axis 1 and 3 are higher than

those of Axis 2 and 4. For the single-frames along the slope direction, the new hinges of beams and columns are mainly found at the elements of floors under the upper-embedding end. While, the number and degree are less than those at the single-frames across the slope direction. Moreover, the non-embedding columns of the upper-embedding story are not damaged. Meanwhile, column hinges at the lower-embedding side of the 4th floor and the upper-embedding side of the 3rd floor are more severe than the other columns.

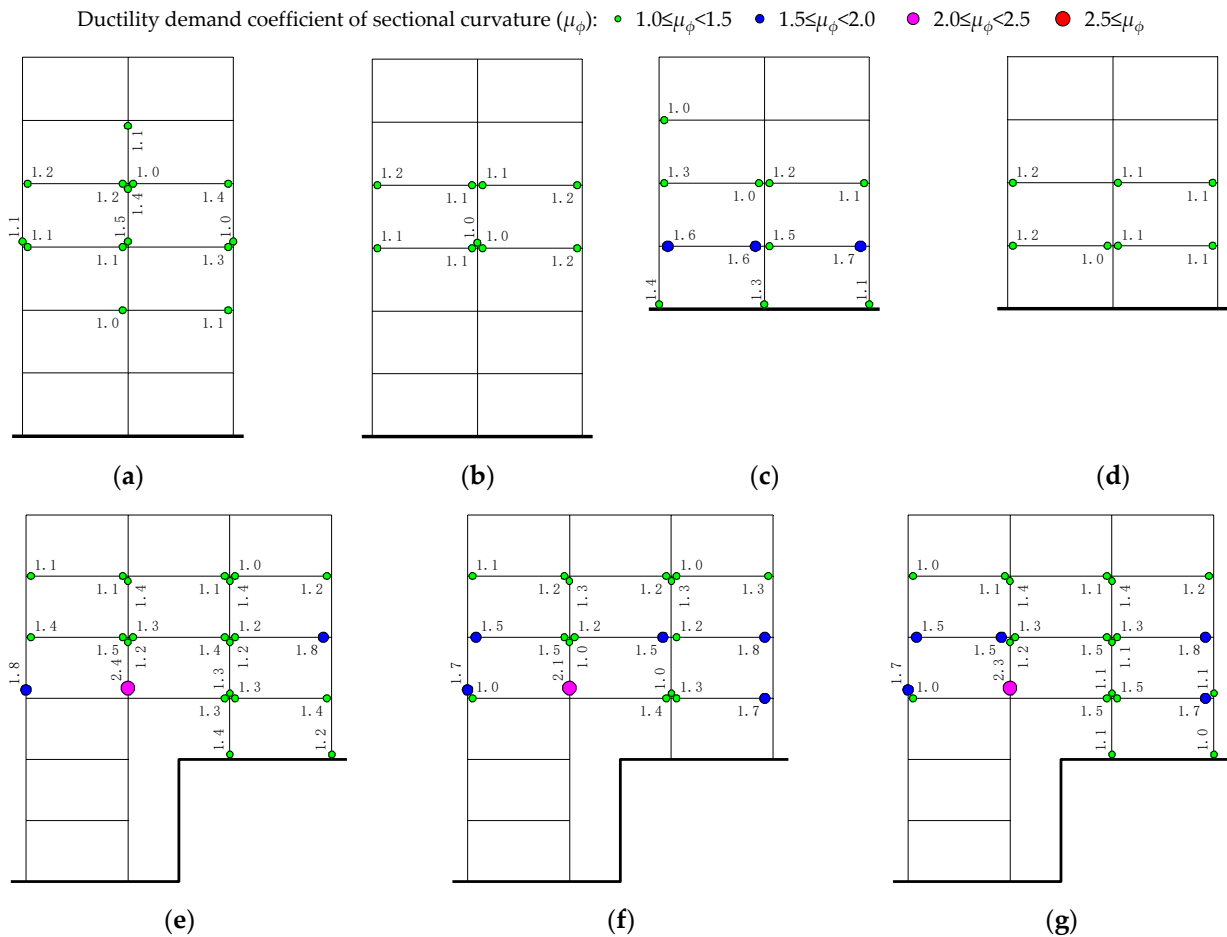


Figure 11. Plastic hinges of the structure under natural wave 2 with seismic intensity of 0.4 g: (a) Axis 1; (b) Axis 2; (c) Axis 3; (d) Axis 4; (e) Axis A; (f) Axis B; (g) Axis C.

With the increase in seismic intensity, plastic hinges occur at the end of beams and columns on floors under the upper-embedding end, revealing that the structural damage has transferred from the beams and columns above the upper-embedding end to those under the upper-embedding end. In addition, the elements on the floors above the upper-embedding end suffered severer damage during the earthquake, e.g., the border upper-embedding columns along the slope direction, innermost upper-embedding columns across the slope direction, beams connected with the upper-embedding column, and columns at the lower-embedding side of the adjacent floor above the upper-embedding story.

It can be seen that the damage of the MBS starts from the floors above the upper-embedding end, then proceeds to the floors under the upper-embedding end. Generally, the failure process of the MBS can be summarized as that part of the beams and columns at the floors above the upper-embedding end firstly yield plastic hinges; subsequently, part of the upper-embedding columns become hinged; then, most of the beams and columns at the floors above the upper-embedding end is damaged; finally, the beams and columns at the floors under the upper-embedding end are damaged. The development of plastic hinges is consistent with the damage phenomenon of shaking table test [21].

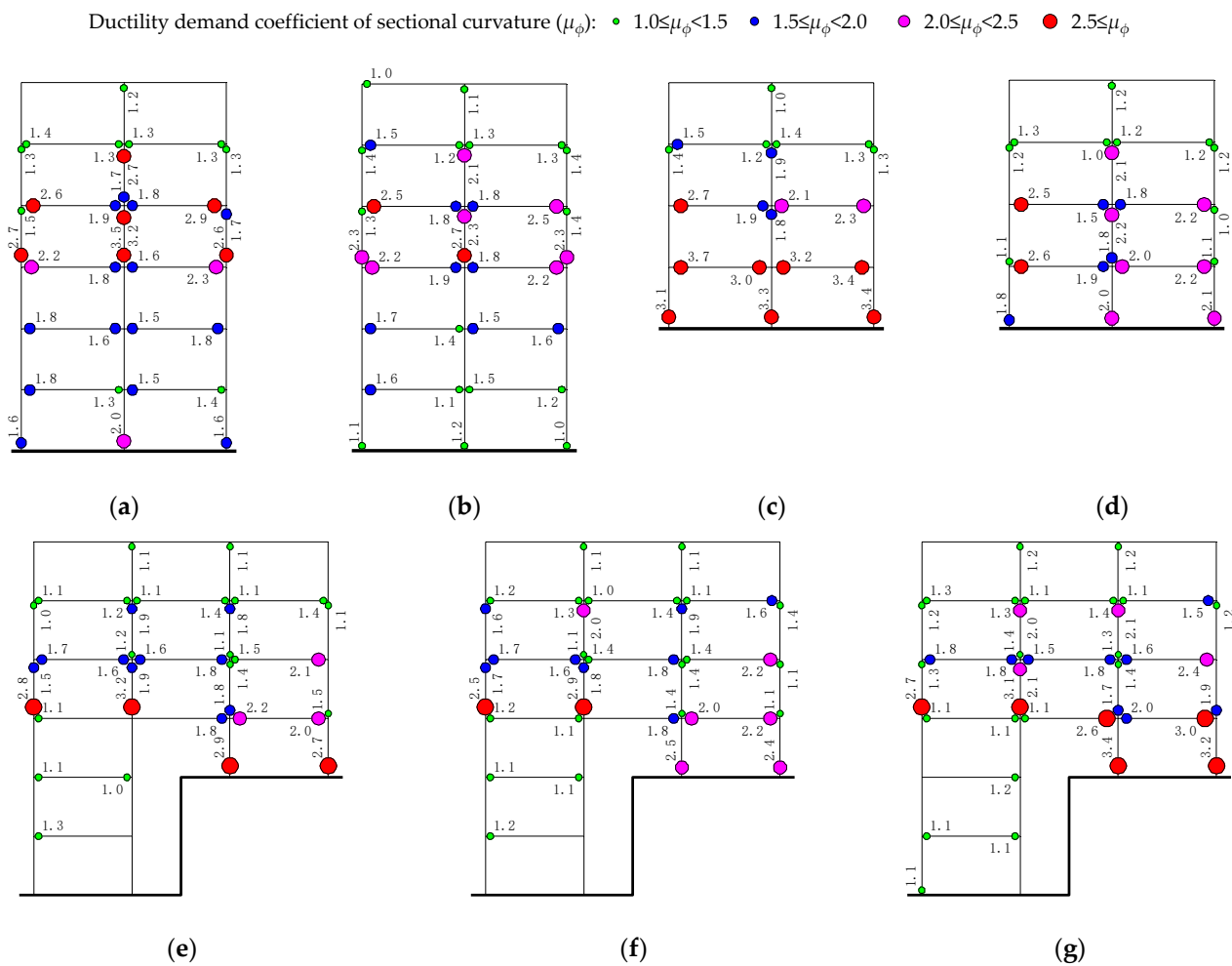


Figure 12. Plastic hinges of the structure under natural wave 2 with seismic intensity of 0.62 g: (a) Axis 1; (b) Axis 2; (c) Axis 3; (d) Axis 4; (e) Axis A; (f) Axis B; (g) Axis C.

Due to the torsional effect, the damage of the border upper-embedding columns along the slope direction and the innermost upper-embedding columns across the slope direction is severer than other upper-embedding columns. The damages of the upper-embedding story and the adjacent upper story are unevenly distributed, and the heavily damaged columns are found in opposite positions. The torsional effect makes the lower-embedding column more prone to hinge across the slope direction.

4. Influence of Stiffness Ratio

4.1. Proposed Nominal Stiffness Ratio

In practical engineering, both the site conditions and the building scheme determine the plane arrangement and the proportion of the plan occupied by the upper- and lower-embedding sides. When the vertical members are uniformly distributed, the proportion of the plan occupied by the upper- and lower- embedding side determines the distribution of stiffness in the upper-embedding story. The stiffness distribution on the upper- and lower- embedding sides of the upper-embedding story will significantly affect the dynamic response of MBS, which should be investigated.

In the upper-embedding story, the stiffness of elements at lower-embedding sides is denoted as k_{p+1}^0 and the stiffness of elements at upper-embedding side is denoted as k_{p+1}^2 . The nominal intra-story stiffness ratio, γ_{intra} , is defined to present the stiffness distribution, and it can be calculated as Equation (2). For MBS, the stiffness of elements at lower-embedding side could be weakened by the deformation of floors under the upper-

embedding end, and the degree of weakening depends on the floor number and lateral stiffness of each floor. Assuming that the layout of floors under the upper-embedding end is the same to simplify the analysis, the lateral stiffness of the adjacent lower floor of the upper embedding story is denoted as k_p , so the nominal below-story stiffness ratio, γ_{below} , is defined as Equation (3).

$$\gamma_{\text{intra}} = \frac{k_{p+1}^0}{k_{p+1}^0 + k_p^2} \quad (2)$$

$$\gamma_{\text{below}} = \frac{k_p}{k_{p+1}^0} \quad (3)$$

4.2. Structure Models

Assuming that the γ_{below} is 0.9, and there are two floors under the upper-embedding end. The γ_{intra} is assigned different values to analyze the effect of the increasing nominal intra-story stiffness ratio.

The total number of frame spans at Axis x and Axis y are 5 and 2, respectively. The total floor number, load distribution, and design basis are the same as model M0, while the number of the spans at axis x on floors under the upper-embedding end and the cross-section of beams and columns are changed and shown in Table 3. The concrete strength grade is C30, except as listed in Table 3. The nominal intra-story stiffness ratio γ_{intra} , eccentricity ratio e/r , and structural period are listed in Table 4, where e is the stiffness eccentricity and r is the radius of gyration of the deck. It should be noted that the γ_{intra} varies simultaneously in both horizontal directions, and e/r along the slope direction inevitably changes.

Table 3. The layout of structure models.

Model ID	Span Number at Axis x on the 1st and 2nd Floor	Cross-Section of Columns/mm \times mm	Cross-Section of Beams/mm \times mm
M1	1	Axis 1,2 of 1st to 3rd floor: 650 \times 700; others: 600 \times 600.	1st to 2nd floor: 300 \times 600; 3rd to 6th floor: Axis x : 250 \times 600; Axis y : 300 \times 600.
M2	2	Axis 1: 550 \times 750; others: 600 \times 600.	Axis x : 250 \times 600; Axis y : 300 \times 600.
M3	3	600 \times 800; (Axis A, C of 3rd floor: C35). 1st~2nd floor: 750 \times 900;	Axis x : 250 \times 600; Axis y : 300 \times 600.
M4	3	Axis 1, 2 of 3rd floor: 750 \times 900; others: 550 \times 800; (Axis A, C of 3rd floor: C35). 1st~2nd floor: 900 \times 800;	1st to 3rd floor: 300 \times 600; 4th to 6th floor: Axis x :250 \times 600; Axis y :300 \times 600.
M5	3	Axis 1, 2 of 3rd floor: 900 \times 800; others: 500 \times 800; (Axis A, C of 3rd floor: C35).	Axis x : 1st to 3rd floor:350 \times 600; 4th to 6th floor:250 \times 600; Axis y : 350 \times 600.
M6	4	Axis 1 to 5 of 1st to 3rd floor: 850 \times 900; others: 700 \times 700; (Axis 6 of 3rd floor: C40).	1st to 3rd floor: 400 \times 600; 4th to 6th floor: 300 \times 600.

Table 4. Parameter of structure models.

Model ID	γ_{intra}		e/r	Period/s			Story Drift/rad	
	Axis x	Axis y	Axis x	T_1	T_2	T_3	Axis x	Axis y
M1	0.19	0.15	0.46	0.55	0.54	0.46	1/590	1/546
M2	0.28	0.24	0.62	0.60	0.54	0.45	1/615	1/545
M3	0.40	0.30	0.73	0.63	0.53	0.42	1/626	1/550
M4	0.50	0.32	0.71	0.60	0.54	0.42	1/597	1/546
M5	0.59	0.36	0.68	0.58	0.55	0.42	1/583	1/564
M6	0.75	0.62	0.54	0.60	0.49	0.43	1/603	1/545

4.3. The Redistribution of Internal Force

The load cases are the same as the example model M0, and the distribution of base-shear, the average λ of lower-embedding columns, floors, and columns on different axes under the action of 4 groups of earthquake waves are analyzed in this section.

4.3.1. Base Shear

The average proportion of base shear along the slope direction and across the slope direction borne by lower-embedding columns are listed in Tables 5 and 6.

Table 5. The average proportion of base shear along the slope direction is borne by lower-embedding columns.

Model ID	γ_{intra}	Seismic Intensity				
		0.07 g	0.2 g	0.4 g	0.51 g	0.62 g
M1	0.19	0.038	0.052	0.121	0.125	0.141
M2	0.28	0.090	0.086	0.185	0.205	0.220
M3	0.40	0.130	0.303	0.395	0.441	0.438
M4	0.50	0.222	0.255	0.354	0.408	0.416
M5	0.59	0.331	0.359	0.443	0.481	0.478
M6	0.75	0.365	0.431	0.470	0.557	0.617

Table 6. The average proportion of base shear across the slope direction is borne by lower-embedding columns.

Model ID	γ_{intra}	Seismic Intensity				
		0.07 g	0.2 g	0.4 g	0.51 g	0.62 g
M1	0.15	0.120	0.113	0.159	0.163	0.176
M2	0.24	0.277	0.312	0.319	0.321	0.325
M3	0.30	0.457	0.595	0.539	0.552	0.541
M4	0.32	0.531	0.595	0.568	0.546	0.572
M5	0.36	0.559	0.613	0.555	0.567	0.559
M6	0.62	0.688	0.785	0.785	0.730	0.720

As can be seen from these tables, the proportion of base shear borne by lower-embedding columns tends to increase with the increase in the γ_{intra} . In addition, the proportion of the base shear borne by lower-embedding columns of each model tends to increase as the seismic intensity increases, and there is normally a redistribution of base shear borne by different embedding columns.

The average λ of lower-embedding columns is presented in Figure 13. It can be seen from Figure 13 that as the γ_{intra} increases, the average λ tends to decrease in both the horizontal directions with the same seismic intensity, indicating that the larger the lateral stiffness of the lower-embedding side members, the less significant the redistribution of base shear in both horizontal directions. Therefore, the less the lateral stiffness of the members at the lower-embedding side, the more necessary it is to consider the effect of this

redistribution of base shear at different embedding ends. For a structure with a greater γ_{intra} , the degree of redistribution of the base shear is less obvious.

4.3.2. Story Shear

The average λ of floors at $a_{PG,x}$ of 0.4 g and 0.62 g are shown in Figures 14 and 15, respectively. It is clear that the average λ trends to increase in both horizontal directions as $a_{PG,x}$ increases. Along the slope direction, for floors above the upper-embedding end, e.g., from the 3rd floor to the 6th floor, the average λ is similar and is independent of the stiffness distribution of the upper-embedding story. For floors under the upper-embedding end, e.g., from the 1st floor to the 2nd floor, the average λ is significantly different with an increasing-decreasing tendency with the increase in γ_{intra} . This indicates that the λ on floors under the upper-embedding end tends to be stable with the increase in the lateral stiffness of elements at the lower-embedding side.

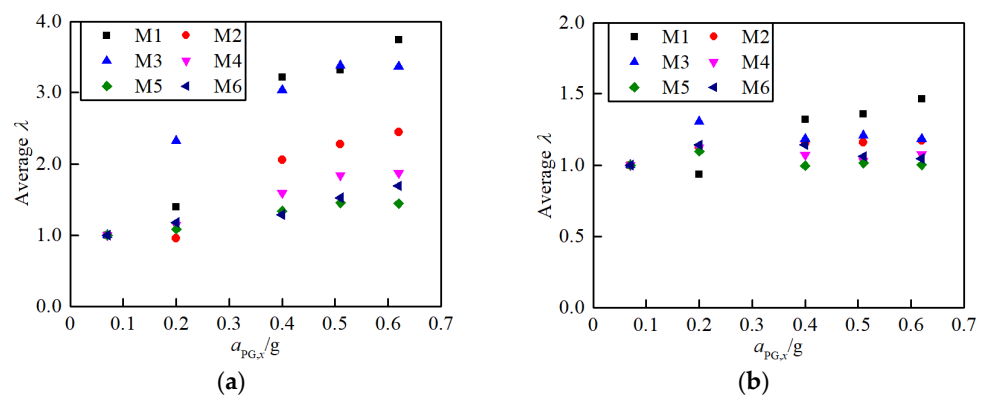


Figure 13. The average λ of lower-embedding columns: (a) Along the slope direction; (b) Across the slope direction.

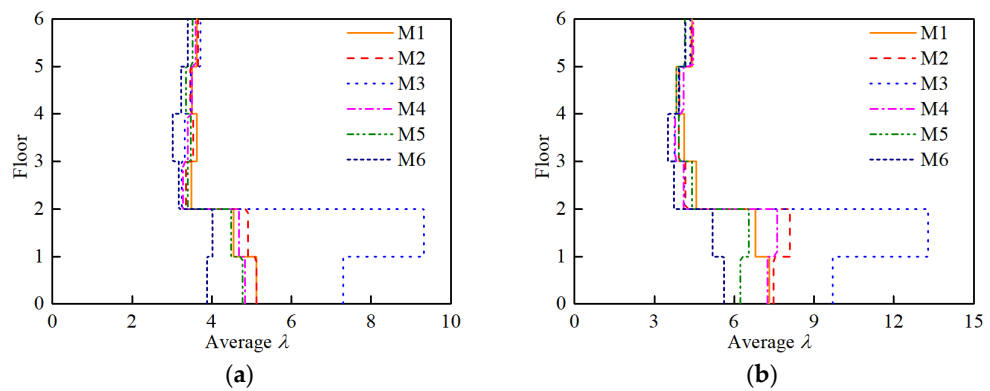


Figure 14. The average λ of floors along the slope direction: (a) $a_{PG,x} = 0.4$ g; (b) $a_{PG,x} = 0.62$ g.

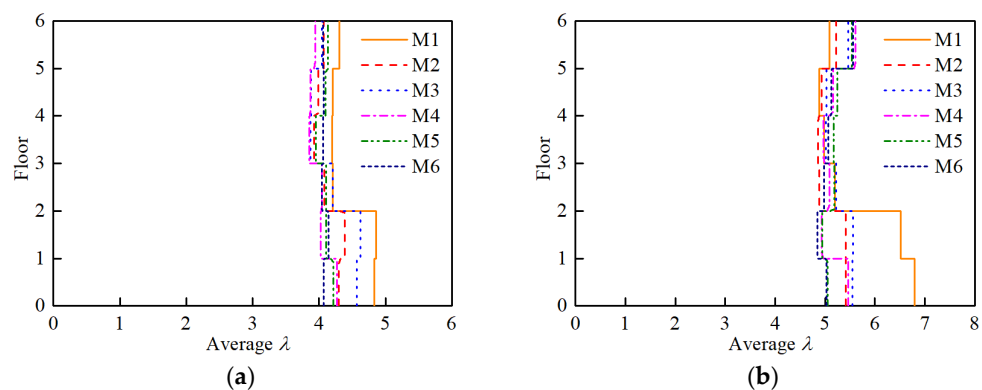


Figure 15. The average λ of floors across the slope direction: (a) $a_{PG,x} = 0.4$ g; (b) $a_{PG,x} = 0.62$ g.

For the story shear across the slope direction, the distribution pattern of average λ on floors above the upper-embedding end is consistent with that along the slope direction, while the distribution pattern of average λ on floors under the upper-embedding end is different from that along the slope direction. At floors under the upper-embedding end, the average λ across the slope direction is obviously less than that along the slope direction with the same seismic intensity, and the average λ tends to decrease as γ_{intra} increases. When γ_{intra} increases to a certain extent, λ of floors under the upper embedding end is close to that of the floors above the upper embedding end.

4.3.3. Column Shear

The average λ of columns at different axes from the 1st floor to the 4th floor at $a_{PG,x}$ of 0.62 g is presented in Table 7. The maximum average λ of the lower-embedding columns is larger than that of the upper-embedding columns. For each model, the maximum average λ of the upper-embedding columns along the slope direction is less than that across the slope direction. Meanwhile, the maximum average λ of the upper-embedding columns decreases and then increases from model M1 to model M6.

Table 7. The average λ of columns along and across the slope direction at $a_{PG,x}$ of 0.62 g.

Model ID	Floor	Along the Slope Direction						Across the Slope Direction					
		Axis 1	Axis 2	Axis 3	Axis 4	Axis 5	Axis 6	Axis 1	Axis 2	Axis 3	Axis 4	Axis 5	Axis 6
M1	4	4.0	4.3	4.1	3.9	3.8	3.0	3.8	4.2	4.0	4.3	4.3	4.0
	3	2.9	4.9	4.2	4.2	4.4	4.2	4.8	4.4	4.2	4.4	5.0	3.2
	2	3.2	3.3	—	—	—	—	4.6	4.3	—	—	—	—
	1	4.7	6.1	—	—	—	—	5.7	6.5	—	—	—	—
M2	4	3.3	3.8	3.7	4.3	4.0	3.0	3.5	3.8	4.1	3.7	4.6	3.8
	3	3.5	6.8	5.1	3.8	4.1	3.8	4.2	4.1	4.5	4.1	4.8	3.4
	2	3.0	7.2	3.3	—	—	—	4.4	4.4	4.1	—	—	—
	1	4.9	7.8	6.2	—	—	—	5.0	5.3	5.4	—	—	—
M3	4	2.9	3.4	3.4	3.3	4.2	2.8	3.6	3.9	4.4	4.7	3.3	3.9
	3	4.2	9.5	9.7	8.2	2.8	2.7	4.8	4.4	4.7	5.2	3.9	3.8
	2	5.4	10.7	11.1	5.7	—	—	4.6	5.0	5.0	4.7	—	—
	1	6.2	9.3	9.7	8.1	—	—	5.2	5.0	5.7	6.4	—	—
M4	4	3.2	3.3	3.3	3.2	5.4	3.8	3.8	4.1	4.3	4.2	3.8	4.2
	3	3.4	6.3	6.3	5.6	3.5	3.5	4.0	3.9	4.1	4.6	4.2	4.4
	2	3.8	6.4	6.7	4.3	—	—	4.0	4.5	4.7	4.6	—	—
	1	4.9	7.0	7.2	6.4	—	—	5.0	4.7	5.3	6.4	—	—
M5	4	3.0	3.7	3.8	3.7	5.0	3.6	3.6	4.3	4.5	4.6	3.8	4.1
	3	3.5	5.7	5.6	4.9	3.6	3.6	4.1	4.0	4.2	4.4	4.3	4.1
	2	3.8	5.8	6.0	4.3	—	—	4.1	4.4	4.5	4.3	—	—
	1	4.4	6.0	6.2	5.6	—	—	4.9	4.6	5.0	5.5	—	—
M6	4	3.2	3.4	3.3	3.3	3.2	2.3	4.0	4.2	4.4	4.5	4.3	4.5
	3	3.2	5.0	5.1	5.1	5.1	2.8	3.9	4.0	4.1	4.3	4.4	4.7
	2	3.5	4.9	5.0	5.1	4.0	—	4.1	4.4	4.5	4.5	4.4	—
	1	4.2	5.3	5.5	5.8	5.4	—	4.9	4.5	4.6	5.2	6.0	—

The average λ of columns at Axis 1 and Axis 2 on the 1st floor of models are shown in Figures 16 and 17, respectively. As can be seen from Figure 16, the average λ of columns along the slope direction at different axes of the 1st floor tends to increase and then decrease with the increase in γ_{intra} at the same seismic intensity, which is consistent with the distribution of the average λ of the 1st floor. And the average λ of the column at axis 2 is greater than that of the column at axis 1. Meanwhile, the average λ of column across the slope direction at different axes of the 1st floor tends to decrease with the increase in γ_{intra} at the same seismic intensity, and the decreasing trend is more obvious at axis 2.

When the stiffness distribution of the upper-embedding story changes, the redistribution of shear force of base, story, and column are different. With the increase in γ_{intra} , the λ of lower embedding-columns tends to decrease significantly along the slope direction, while the λ of floors under the upper-embedding end and the column on the 1st floor both first increase and then decrease. This is because the base shear is borne by upper- and lower- embedding columns, while the story shear of floors under the upper-embedding end and shear of columns on the 1st floor are mainly related to lower-embedding columns. The shear redistribution at different floors is detrimental to the seismic resistance of the structure, and the most significant degree of shear redistribution at different floors occurs when γ_{intra} increases to a certain degree.

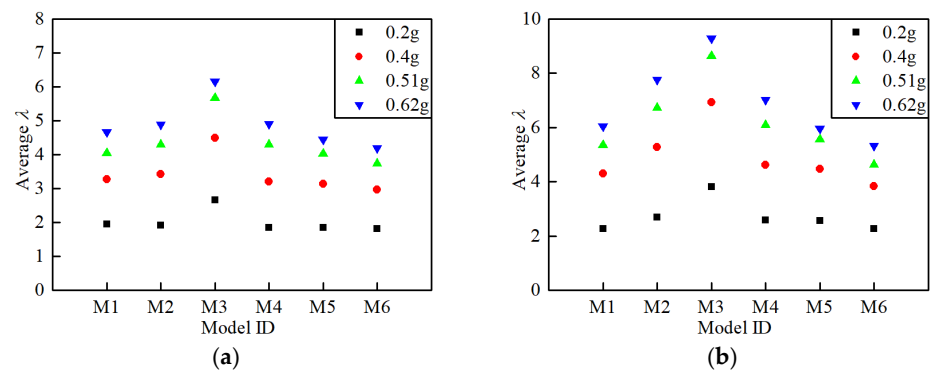


Figure 16. The average λ of columns along the slope direction on the 1st floor: (a) Axis 1; (b) Axis 2.

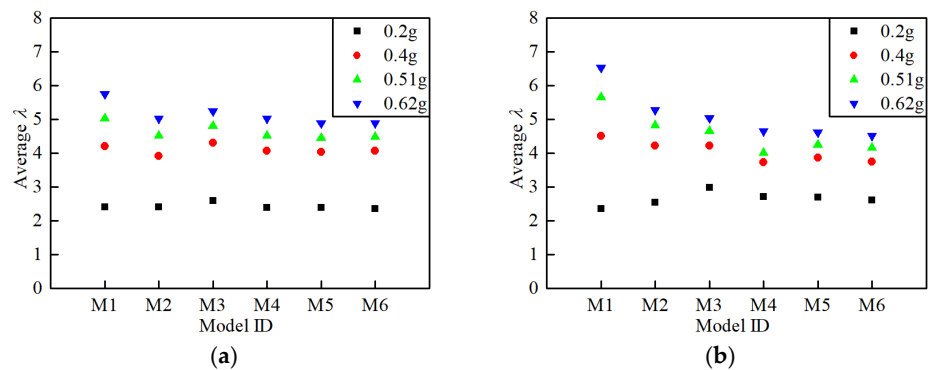


Figure 17. The average λ of columns across the slope direction on the 1st floor: (a) Axis 1; (b) Axis 2.

4.4. Distribution and Development of Plastic Hinges

The distribution of the plastic hinge of the single-frame at Axis B under seismic action of the artificial wave with the intensity of 0.62 g is shown in Figure 18.

For structure models M1, M2, M3, and M6 with different geometric arrangements, the larger the γ_{intra} , the more severe the damage to the upper-embedding column. When the γ_{intra} is small, the number and degree of plastic hinges at the end of columns on the 4th to 5th floor are relatively large, and the damage of structural members is relatively uniform. However, when the γ_{intra} is relatively large, the damage of the upper-embedding column is more severe than that of other members, and the damage is concentrated.

For the structure models M3, M4, and M5 with the same geometric arrangement, the sections of elements in the upper-embedding story and floors under the upper-embedding end are adjusted to obtain different γ_{intra} . Meanwhile, the sections of columns at Axis 1, 2, 3, and 4 on the 4th floor in models M4 and M5 are reduced compared with columns at the same positions on the upper-embedding story. The D-value method is used to calculate the lateral stiffness of the members, and the lateral stiffness ratio of non-embedding columns in the upper-embedding story to the corresponding members in the adjacent upper story is defined as the corresponding stiffness ratio γ_{non} , whose values are 0.94, 1.14 and 1.33 for

the three structures, respectively. Comparing the plastic hinge of these three structures, it can be seen that increasing the lateral stiffness of floors under the upper-embedding end and non-embedding columns makes γ_{intra} increase, while the γ_{non} increases, the degree of plastic hinge of the upper-embedding column weakens, the damage degree of columns adjacent above the non-embedding column increases, and the damage at floors above the upper-embedding end is aggravated. When the stiffness of non-embedding members and floors under the upper-embedding end is enhanced, the damage of the upper-embedding column is mitigated, and the structural damage is transferred to the upper floors, which is contrary to the law of structures with different geometric arrangements. This also indicates that the damage to the upper-embedding column is related to the relative stiffness of non-embedding columns and the corresponding member in the adjacent upper story.

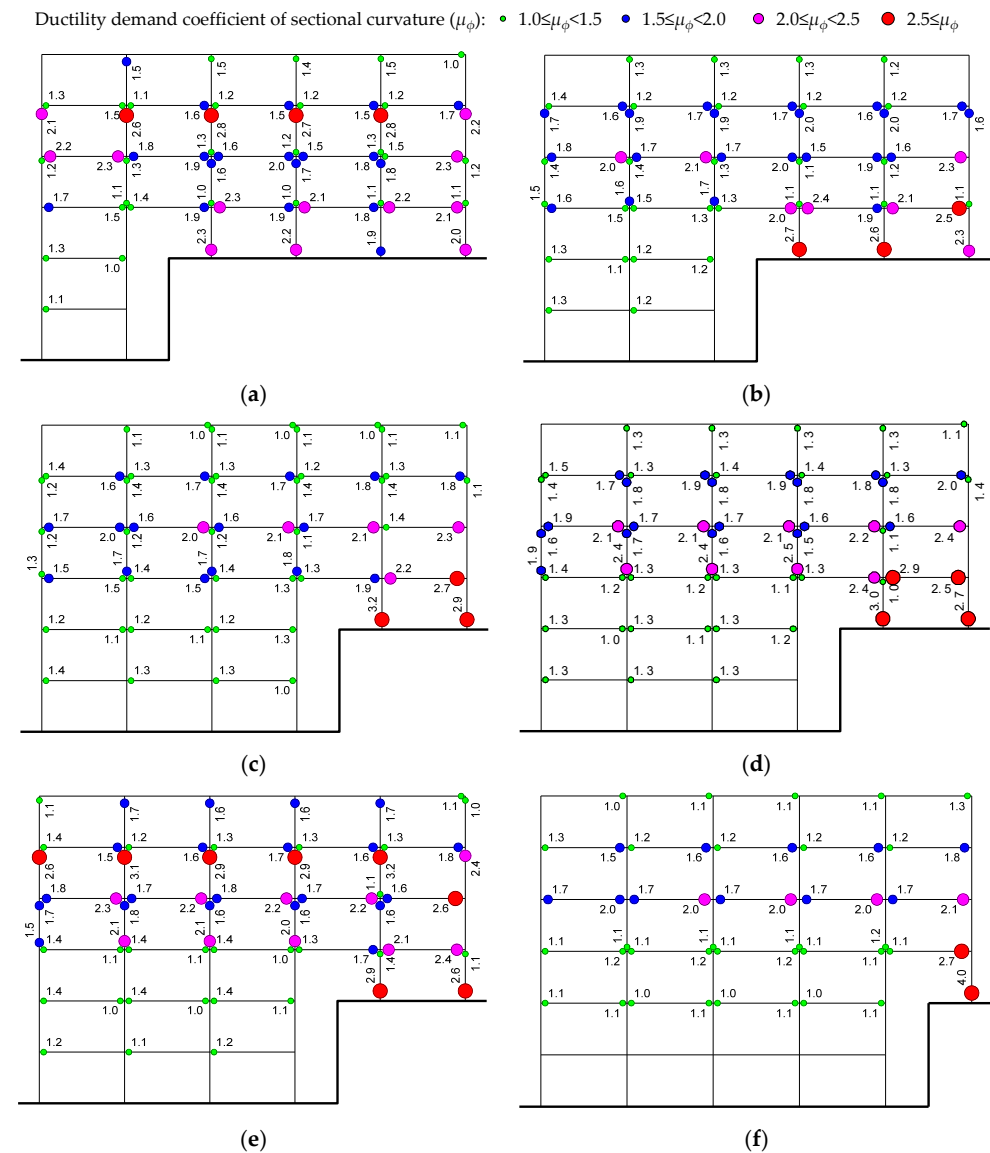


Figure 18. Plastic hinges of the single-frame at Axis B: (a) M1; (b) M2; (c) M3; (d) M4; (e) M5; (f) M6.

The influence factor of plastic hinge degree is complex. When γ_{intra} increases with increasing elements at the lower-embedding side and reducing elements at the upper-embedding side, damage tends to be formed in the upper-embedding column. When γ_{intra} increases with the increasing lateral stiffness of non-embedding columns and elements on floors under the upper-embedding end, the damage of upper-embedding columns is weakened, and the damage of columns on upper floors is aggravated. When γ_{intra}

is relatively large, the damage forms in upper-embedding columns and the connected beams. Therefore, some measures can be taken to improve the drift ductility of the upper-embedding column, such as setting the upper-embedding column as a highly ductile fiber-reinforced concrete column [33] or a steel column, or reducing the drift ductility requirement, such as weakening the degree of restraint at the bottom to enhance safety.

The plastic hinge across the slope direction varies considerably for structures with different γ_{intra} . The plastic hinge distribution of the single-frame at Axis 1 is shown in Figure 19. It can be seen that the degree of the plastic hinge of the single-frame is: model M1 < model M2 < model M6 < model M3, which is consistent with the eccentricity ratio e/r of models. This shows that the damage degree of the frame at the lower-embedding side is significantly influenced by the torsion effect as the greater the torsion effect, the more severe the damage to the frame across the slope direction of the structure.

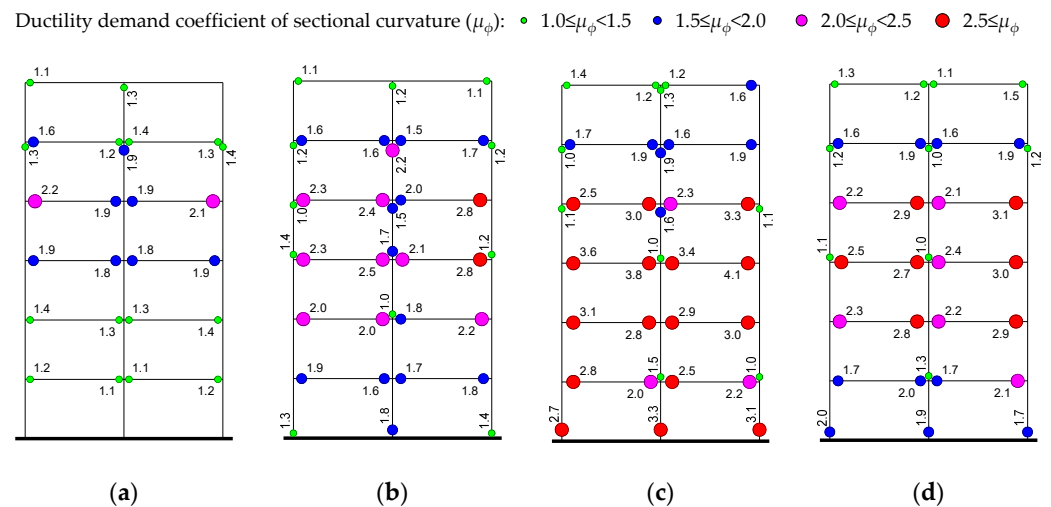


Figure 19. Plastic hinges of the single-frame at Axis 1: (a) M1; (b) M2; (c) M3; (d) M6.

The hinge rates of the beams and columns continue to increase with increasing seismic intensity. The average hinge rates for the model beams and columns at different levels under 0.4 g and 0.62 g seismic action are shown in Figures 20–22. For structure models M1, M2, M3 and M6 with different geometric arrangements, as γ_{intra} increases, the average hinge rate along the slope direction of the column decreases significantly, and the rate of μ_ϕ in the range of $[3.0, +\infty)$ decreases. However, for structure models M3, M4, and M5 with the same geometric arrangement, the average hinge rate along the slope direction of the column gradually increases with the increasing γ_{intra} , and the rate of μ_ϕ reaches $[3.0, +\infty)$ increases, which is consistent with the opposite distribution pattern of the plastic hinge as depicted above. The distribution of hinge rate across the slope direction of the column has a noticeable change with increasing seismic intensity. The relationship between the distribution of column hinge rate across the slope direction and the variation of γ_{intra} and e/r is not apparent when the seismic intensity is 0.4 g. Under the earthquake intensity of 0.62 g, the variation law of the column hinge rate across the slope direction is similar to that along the slope direction, but the rate of μ_ϕ reaching $[3.0, +\infty)$ is smaller than that along the slope direction. For beams, the average hinge rate tends to decrease and then increase with increasing γ_{intra} under the earthquake action of 0.4 g. As the seismic intensity increases to 0.62 g, the pattern of the average hinge rate at the beam end changes, increasing and then decreasing with the increasing γ_{intra} , but the rate of μ_ϕ reaching $[3.0, +\infty)$ is closer.

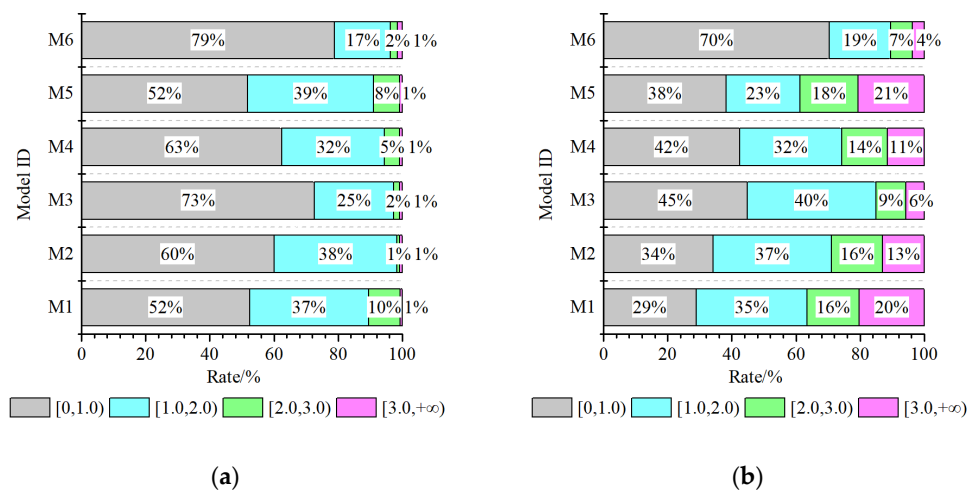


Figure 20. The average column hinge rate along the slope direction: (a) $a_{PG,x} = 0.4$ g; (b) $a_{PG,x} = 0.62$ g.

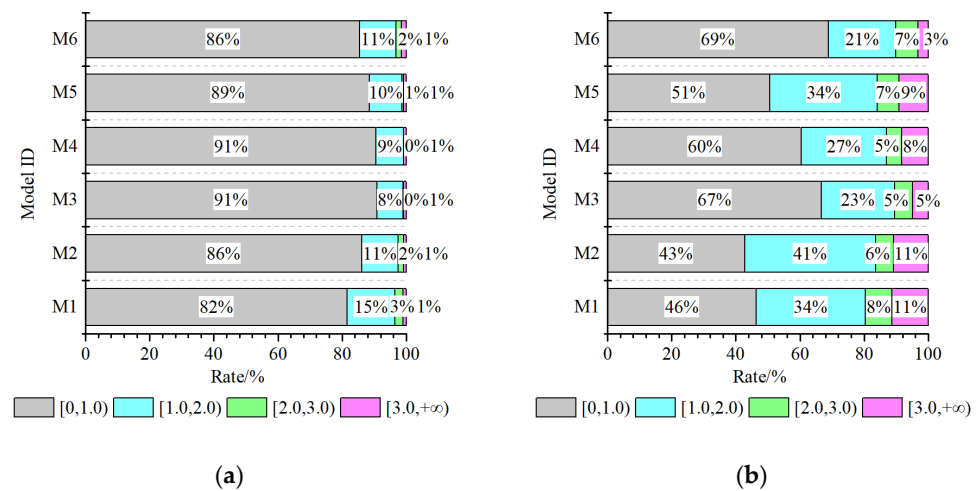


Figure 21. The average column hinge rate across the slope direction: (a) $a_{PG,x} = 0.4$ g; (b) $a_{PG,x} = 0.62$ g.

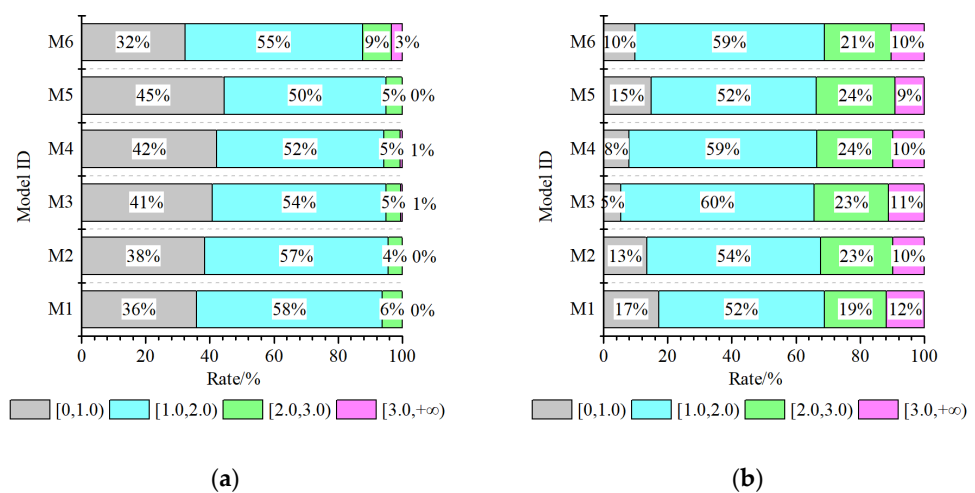


Figure 22. The average beam hinge rate: (a) $a_{PG,x} = 0.4$ g; (b) $a_{PG,x} = 0.62$ g.

5. Conclusions

The seismic response of the MBS differs from that of ordinary structures, and the former suffers from severe torsional effects. While most previous studies focus on the seismic failure mechanism of the plan along the slope direction and its final damage state,

the research on the structural force is simple. In this paper, the time history analysis of three-dimensional MBSs was conducted, considering the torsional effects. The internal force and plastic hinge of the MBSs were concerned, including the redistribution of the shear force of the base, story, and column, and the distribution and development of the plastic hinges. Also, the nominal intra-story stiffness ratio γ_{intra} was proposed as a parameter to study its influence on the redistribution of internal forces and the development of plastic hinges. Conclusions can be drawn as follows:

- (a) The redistribution of the base shear of MBS was evident at different embedding ends, and the redistribution of story shear at different floors also took place. The changes in λ of the columns at Axis 1 and Axis 2 are different from those at Axis 3 and Axis 4 on the upper-embedding story and the adjacent upper floor, and the λ of columns on the 1st floor is greater than that of the adjacent upper story. Moreover, the change trend of λ of the MBS is more prominent along the slope direction.
- (b) On the damage path of MBS, the damage has been transferred from the floors above the upper-embedding end to the floors under the upper-embedding end, where the elements of the floors above the upper-embedding end were the most heavily damaged. Additionally, the damage in both the upper-embedding story and the adjacent upper story are unevenly distributed, and the heavily-damaged columns are in opposite positions. The torsional effect makes the lower-embedding column more prone to hinge across the slope direction.
- (c) When γ_{below} is 0.9, and the number of floors under the upper-embedding end is 2, the redistributions of the shear force of the base, story, and column vary with γ_{intra} . A larger γ_{intra} would result in a weaker redistribution of the base shear in both two horizontal directions. With the increase in γ_{intra} , the redistribution of the story shear along the slope direction at the floors under the upper-embedding end tends to be enhanced and then weakened, where the redistribution was the most serious when γ_{intra} was 0.4. For single-frames across the slope direction, the redistribution of the story shear at the floors under the upper-embedding end tends to be weakened as γ_{intra} increases. The λ of columns on the 1st floor is consistent with the distribution of the λ of the 1st floor. Therefore, the redistribution of the internal force of MBS should be considered in practical seismic design.
- (d) The forming of the plastic hinge of single-frames along the slope direction is related to γ_{intra} and γ_{non} . When γ_{intra} increases and γ_{non} is constant, the damage tends to concentrate on the upper-embedding columns. When γ_{intra} increases with the increase in γ_{non} , the damage of the upper-embedding column is weakened, and the damage of columns on the upper floors is enhanced. The damage degree of single-frames across the slope direction is significantly influenced by the torsional effect.
- (e) The load-bearing capacity and drift ductility of the upper-embedding columns should be improved to avoid serious damage under earthquakes, and the upper-embedding column could be set as a highly ductile fiber-reinforced concrete column or a steel column. The shear bearing capacity of the vertical members of floors under the upper-embedding end can be increased to bear the increased shear force.

There are also some limitations in this study, such as the number of floors under and above the upper-embedding end, the stiffness ratio of floors under the upper-embedding end to the upper-embedding story is taken as constant values, and the effect of the stiffness ratio of the upper-embedding story to the adjacent upper story is not considered. Further research could be conducted into the influence of these factors.

Author Contributions: Conceptualization, Y.T. and S.J.; Data curation, B.J. and S.J.; Formal analysis, B.J. and S.J.; Funding acquisition, Y.L.; Methodology, Y.T. and S.J.; Software, Y.T.; Supervision, Y.L. and L.W.; Writing—original draft, Y.T., B.J. and S.J.; Writing—review & editing, Y.T., Y.L., B.J., L.W. and S.J. All authors have read and agreed to the published version of the manuscript.

Funding: This research was funded by the National Natural Science Foundation of China (Nos. 51638002, 51878101 and 52278484).

Institutional Review Board Statement: Not applicable.

Informed Consent Statement: Not applicable.

Data Availability Statement: The data used to support the findings of this study are available from the corresponding author on reasonable request.

Acknowledgments: The authors sincerely thank Peiyuan Chen for his help revising the paper.

Conflicts of Interest: The authors declare no conflict of interest. The funders had no role in the design of the study; in the collection, analyses, or interpretation of data; in the writing of the manuscript; or in the decision to publish the results.

References

1. Li, Y.; Liu, L. *Building Damage and Thinking of Wenchuan Earthquake*, 1st ed.; Chongqing University Press: Chongqing, China, 2008; pp. 118–128.
2. Narayanan, A.R.V.; Goswami, R.; Murty, C.V.R. Performance of RC buildings along hill slopes of Himalayas during 2011 Sikkim Earthquake. In Proceedings of the 15th World Conference of Earthquake Engineering, Lisboa, Portugal, 24–28 September 2012.
3. Singh, Y.; Gade, P.; Lang, D.H.; Erduran, E. Seismic behavior of buildings located on slopes—An analytical study and some observations from Sikkim Earthquake of September 18, 2011. In Proceedings of the 15th World Conference of Earthquake Engineering, Lisboa, Portugal, 24–28 September 2012.
4. Surana, M.; Singh, Y.; Lang, D.H. Seismic characterization and vulnerability of building stock in hilly regions. *Nat. Hazards Rev.* **2018**, *19*, 4017024. [[CrossRef](#)]
5. Surana, M.; Singh, Y.; Lang, D.H. Fragility analysis of hillside buildings designed for modern seismic design codes. *Struct. Design Tall Spec. Build.* **2018**, *27*, e1500. [[CrossRef](#)]
6. Birajdar, B.G.; Nalawade, S.S. Seismic analysis of buildings resting on sloping ground. In Proceedings of the 13th World Conference on Earthquake Engineering, Vancouver, BC, Canada, 1–6 August 2004.
7. Chhetri, S.; Adhikari, S. Seismic performance of step back, step back set back and set back buildings in sloping ground base. *Struct. Mech. Eng. Constr. Build.* **2021**, *17*, 538–547. [[CrossRef](#)]
8. Tang, Y.Y.; Li, Y.M.; Ji, S.Y.; Liu, L.P. Comparative analysis of seismic performance between step-back frame structure and common frame structure. In Proceedings of the 17th World Conference on Earthquake Engineering, Sendai, Japan, 27 September–2 October 2021.
9. Yang, Y.; Wang, Y.; Li, Y. Study on seismic resistance behavior of the frame connected with ground by not only the first floor. *J. Vib. Shock* **2007**, *26*, 36–40.
10. Tang, Y.; Li, Y.; Huang, Z.; Liu, L.; Ding, Y.; Zhu, H. Analysis of local site effect on seismic response of frame structure supported by foundations with different elevations. In Proceedings of the First South Asia Conference on Earthquake Engineering, Karachi, Pakistan, 21–22 February 2019.
11. Li, Y.; Xu, J.; Wang, G. Seismic fragility analysis of RC frames on steep slopes under near-fault and far-field ground motions. In Proceedings of the 16th European Conference on Earthquake Engineering, Thessaloniki, Greece, 18–22 June 2018.
12. Aggarwal, Y.; Saha, S.K. Seismic performance assessment of reinforced concrete hilly buildings with open story. *Structures* **2021**, *34*, 224–238. [[CrossRef](#)]
13. Thakur, A.; Ashish, D.K.; Verma, S.K. Influence of rooftop telecommunication tower on set back-step back building resting on different ground slopes. *Earth Eng. Eng. Vib.* **2019**, *18*, 351–362. [[CrossRef](#)]
14. Li, R.; Liu, L.; Yin, Y.; Zhang, C.; Li, Y. Seismic Performance of RC Split-Foundation Frame Structures with Steel Braces in the Mountainous Area. *Int. J. Str. Stab. Dyn.* **2022**, *22*, 2240011. [[CrossRef](#)]
15. Surana, M.; Meslem, A.; Singh, Y.; Lang, D.H. Analytical evaluation of damage probability matrices for hill-side RC buildings using different seismic intensity measures. *Eng. Struct.* **2020**, *207*, 110254. [[CrossRef](#)]
16. Surana, M.; Singh, Y.; Lang, D.H. Effect of irregular structural configuration on floor acceleration demand in hill-side buildings. *Earthq. Eng. Struct. D* **2018**, *47*, 2032–2054. [[CrossRef](#)]
17. Jain, A.; Surana, M. Floor displacement-based torsional amplification factors for seismic design of acceleration-sensitive non-structural components in torsionally irregular RC buildings. *Eng. Struct.* **2022**, *254*, 113871. [[CrossRef](#)]
18. Xu, J.; Ji, S.Y.; Li, Y.M.; Liu, L.P.; Wang, X.W.; Wang, G.J. Seismic failure modes identification of split-foundation RC frame structures. In Proceedings of the 17th World Conference on Earthquake Engineering, Sendai, Japan, 27 September–2 October 2021.
19. Xu, G.; Li, A.Q. Seismic performance and improvements of stepback steel frames. *J. Earthq. Eng.* **2021**, *25*, 163–187. [[CrossRef](#)]
20. Yang, B. Quasi-Static Experimental Study on Seismic Performance of Typical Mountainous Cliff-Structure. Master's Thesis, Chongqing University, Chongqing, China, 2014.
21. Li, Y.; Tang, Y.; Jiang, B. Shaking table test of RC frame structure on a slope and supported by foundations with different elevations. *J. Build. Struct.* **2020**, *41*, 68–78.
22. Xu, G.; Zhang, R.; Li, A. Seismic performance and improvements of split-foundation buildings in across-slope direction. *Adv. Struct. Eng.* **2020**, *23*, 749–763. [[CrossRef](#)]

23. Kołodziejczyk, E.; Waśniewski, T. Flexural Behaviour and Internal Forces Redistribution in LWAC Double-Span Beams. *Materials* **2021**, *14*, 5614. [[CrossRef](#)] [[PubMed](#)]
24. Winkler, R.; Bours, A.; Walter, A.; Knobloch, M. Redistribution of Internal Torsional Moments Caused by Plastic Yielding of Structural Steel Members. *Structures* **2019**, *17*, 21–33. [[CrossRef](#)]
25. Tian, Y.; Lu, X.; Huang, D.; Wang, T. SCI Effects under Complex Terrains: Shaking Table Tests and Numerical Simulation. *J. Earth Eng.* **2023**, *27*, 1237–1260. [[CrossRef](#)]
26. Ji, S.; Li, Y.; Han, J.; Liu, L.; Cui, J.; Zhao, Y. Study on overturning resistant property of slope with unequal altitude supports under earthquake action. In Proceedings of the 15th World Conference of Earthquake Engineering, Losiba, Portugal, 24–28 September 2012.
27. Wu, C. Study on Seismic Design of Step-Terrace Structure Based on Failure Control. Master’s Thesis, Chongqing University, Chongqing, China, 2017.
28. Jiang, B.; Ji, S.; Li, Y.; Chen, Z.; Tang, Y. Influence of axial beam tension on seismic performance of RC beam-column joints. In Proceedings of the 16th World Conference of Earthquake Engineering, Santiago, Chile, 9–13 January 2017.
29. GB 50011–2010; Code for Seismic Design of Buildings. China Ministry of Construction: Beijing, China, 2010.
30. Qu, Z.; Ye, L. Strength deterioration Model Based on Effective Hysteretic Energy Dissipation for RC Members under Cyclic Loading. *Eng. Mech.* **2011**, *28*, 45–51.
31. Luo, W. Study on Seismic Damage Control-Based Design Methodology for RC Frames. Ph.D. Thesis, Chongqing University, Chongqing, China, 2015.
32. Gaetani d’Aragona, M.; Polese, M.; Elwood, K.J.; Baradaran Shoraka, M.; Prota, A. Aftershock collapse fragility curves for non-ductile RC buildings a scenario-based assessment. *Earthq. Eng. Struct. D* **2017**, *46*, 2083–2102. [[CrossRef](#)]
33. Li, R.; Deng, M.; Zhang, Y. Behavior of highly ductile fiber-reinforced concrete columns under eccentric loading. *Structures* **2021**, *33*, 3357–3370. [[CrossRef](#)]

Disclaimer/Publisher’s Note: The statements, opinions and data contained in all publications are solely those of the individual author(s) and contributor(s) and not of MDPI and/or the editor(s). MDPI and/or the editor(s) disclaim responsibility for any injury to people or property resulting from any ideas, methods, instructions or products referred to in the content.